J. Fluid Mech. (2006), *vol.* 550, *pp.* 349–358.
doi:10.1017/S002211200500844X Printed in the United Kingdom

Acceleration statistics of heavy particles in turbulence

By J. BEC[1], L. BIFERALE[2], G. BOFFETTA[3], A. CELANI[4], M. CENCINI[5], A. LANOTTE[6], S. MUSACCHIO[7] AND F. TOSCHI[8]

[1]CNRS Observatoire de la Côte d'Azur, B.P. 4229, 06304 Nice Cedex 4, France

[2]Department of Physics and INFN, University of Rome "Tor Vergata", Via della Ricerca Scientifica 1, 00133 Roma, Italy

[3]Department of Physics and INFN, University of Torino, Via Pietro Giuria 1, 10125, Torino, Italy

[4]CNRS, INLN, 1361 Route des Lucioles, F-06560 Valbonne, France

[5]SMC-INFM c/o Department of Physics, University of Rome "La Sapienza", Piazz.le A. Moro, 2, I-00185 Roma, Italy, and CNR-ISC via dei Taurini 19, I-00185 Roma, Italy

[6]CNR-ISAC, Sezione di Lecce, Str. Prov. Lecce-Monteroni km 1,200, I-73100 Lecce, Italy

[7]Department of Physics, University of Rome "La Sapienza", Piazz.le A. Moro, 2, I-00185 Roma, Italy

[8]CNR-IAC, Viale del Policlinico 137, I-00161 Roma, Italy and INFN, Sezione di Ferrara, via G. Saragat 1, I-44100, Ferrara, Italy

(Received 5 August 2005 and in revised form 9 December 2005)

We present the results of direct numerical simulations of heavy particle transport in homogeneous, isotropic, fully developed turbulence, up to resolution 512^3 ($R_\lambda \approx 185$). Following the trajectories of up to 120 million particles with Stokes numbers, St, in the range from 0.16 to 3.5 we are able to characterize in full detail the statistics of particle acceleration. We show that: (i) the root-mean-squared acceleration $a_{\rm rms}$ sharply falls off from the fluid tracer value at quite small Stokes numbers; (ii) at a given St the normalized acceleration $a_{\rm rms}/(\epsilon^3/\nu)^{1/4}$ increases with R_λ consistently with the trend observed for fluid tracers; (iii) the tails of the probability density function of the normalized acceleration $a/a_{\rm rms}$ decrease with St. Two concurrent mechanisms lead to the above results: preferential concentration of particles, very effective at small St, and filtering induced by the particle response time, that takes over at larger St.

1. Introduction

Small impurities like dust, droplets or bubbles suspended in an incompressible flow are finite-size particles whose density may differ from that of the suspending fluid, and cannot thus be modelled as point-like tracers. The description of their motion must account for inertia whence the name *inertial particles*. At long times particles concentrate in singular sets evolving with the fluid motion, leading to the appearance of a strong spatial inhomogeneity dubbed *preferential concentration*. At the experimental level such inhomogeneities have long been known (see Eaton & Fessler 1994 for a review) and utilized for flow visualization (e.g. exploiting bubble clustering inside vortex filaments). The statistical description of particle concentration is at present a largely open question with many industrial and environmental applications, such as spray combustion in diesel engines (Post & Abraham 2002) or some rocket propellers (Villedieu & Hylkema 2000), the formation of rain droplets in warm clouds

(Pinsky & Khain 1997; Falkovich, Fouxon & Stepanov 2002; Shaw 2003) or the coexistence of plankton species (Rothschild & Osborn 1988; Lewis & Pedley 2000). Inertial particles are also relevant to spore, pollen, dust or chemicals dispersion in the atmosphere where the diffusion by air turbulence may even be overcome by preferential clustering (Csanady 1980; Seinfeld 1986).

On the experimental side, the study of particle motion in turbulence has recently undergone rapid progress thanks to the development of effective optical and acoustical tracking techniques (La Porta *et al.* 2001, 2002; Mordant *et al.* 2001; Warhaft, Gylfason & Ayyalasomayajula 2005). In parallel with the experimental effort, theoretical analysis (Balkovsky, Falkovich & Fouxon 2001; Falkovich & Pumir 2004; Bec, Gawedzki & Horvai 2004; Zaichik, Simonin & Alipchenkov 2003) and numerical simulations (Boivin, Simonin & Squires 1998; Reade & Collins 2000; Zhou, Wexler & Wang 2001; Chun *et al.* 2005) are paving the way to a thorough understanding of inertial particle dynamics in turbulent flows. Recently, the presence of strong inhomogeneities characterized by fractal and multifractal properties have been predicted, and found in theoretical and numerical studies of stochastic laminar flows (Balkovsky *et al.* 2001; Bec 2004; Bec 2005), in two-dimensional turbulent flows (Boffetta, De Lillo & Gamba 2004) and in three-dimensional turbulent flows at moderate Reynolds numbers in the limit of vanishing inertia (Falkovich & Pumir 2004).

Here we present a direct numerical simulations (DNS) study of particles much heavier than the carrier fluid in high-resolution turbulent flows. In particular, we shall focus on the behaviour of particle acceleration at varying both Stokes and Reynolds numbers. For fluid tracers, it is known that trapping into vortex filaments (La Porta *et al.* 2001; Biferale *et al.* 2005) is the main source of strong acceleration events. On the other hand, little is known about the acceleration statistics of heavy particles in turbulent flows, where preferential concentration may play a crucial role. Moreover, since in most applied cases it is almost impossible to perform DNS of particle transport in realistic settings, it is important to understand acceleration statistics for building stochastic models of particle motion with and without inertia (Sawford & Guest 1991).

2. Heavy particle dynamics and numerical simulations

The equations of motion of a small, rigid, spherical particle immersed in an incompressible flow have been consistently derived from first principles by Maxey & Riley (1983). In the limiting case of particles much heavier than the surrounding fluid, these equations take the particularly simple form

$$\frac{\mathrm{d}\boldsymbol{X}}{\mathrm{d}t} = \boldsymbol{V}(t), \qquad \frac{\mathrm{d}\boldsymbol{V}}{\mathrm{d}t} = -\frac{\boldsymbol{V}(t) - \boldsymbol{u}(\boldsymbol{X}(t), t)}{\tau_s}. \tag{2.1}$$

Here, $\boldsymbol{X}(t)$ denotes the particle trajectory, $\boldsymbol{V}(t)$ its velocity, and $\boldsymbol{u}(\boldsymbol{x}, t)$ is the fluid velocity. The Stokes response time is $\tau_s = 2\rho_p a^2/(9\rho_f \nu)$ where a is the particle radius, ρ_p and ρ_f are the particle and fluid density, respectively, and ν is the fluid kinematical viscosity. The Stokes number is defined as $St = \tau_s/\tau_\eta$ where $\tau_\eta = (\nu/\epsilon)^{1/2}$ is the Kolmogorov timescale and ϵ the average rate of energy injection. Equation (2.1) is valid for very dilute-suspensions, where particle–particle interactions (collisions) and hydrodynamic coupling are not taken into account.

The fluid evolves according to the incompressible Navier–Stokes equations

$$\frac{\partial \boldsymbol{u}}{\partial t} + \boldsymbol{u}\cdot\nabla\boldsymbol{u} = -\frac{\nabla p}{\rho_f} + \nu\Delta\boldsymbol{u} + \boldsymbol{f}, \tag{2.2}$$

where p is the pressure field and $\boldsymbol{f}$ is the external energy source, $\langle \boldsymbol{f}\cdot\boldsymbol{u}\rangle = \epsilon$.

R_λ	$u_{\rm rms}$	ε	ν	η	L	T_E	τ_η	T_{tot}	T_{tr}	Δx	N^3	N_t	N_p	N_{tot}
185	1.4	0.94	0.00205	0.010	π	2.2	0.047	14	4	0.012	512^3	5×10^5	7.5×10^6	12×10^7
105	1.4	0.93	0.00520	0.020	π	2.2	0.073	20	4	0.024	256^3	2.5×10^5	2×10^6	32×10^6
65	1.4	0.85	0.01	0.034	π	2.2	0.110	29	6	0.048	128^3	3.1×10^4	2.5×10^5	4×10^6

TABLE 1. Parameters of DNS. Microscale Reynolds number R_λ, root-mean-square velocity $u_{\rm rms}$, energy dissipation ε, viscosity ν, Kolmogorov lengthscale $\eta = (\nu^3/\varepsilon)^{1/4}$, integral scale L, large-eddy Eulerian turnover time $T_E = L/u_{\rm rms}$, Kolmogorov timescale τ_η, total integration time T_{tot}, duration of the transient regime T_{tr}, grid spacing Δx, resolution N^3, number of trajectories of inertial particles for each St N_t saved at frequency $\tau_\eta/10$, number of particles N_p per St stored at frequency $10\tau_\eta$, total number of advected particles N_{tot}. Errors on all statistically fluctuating quantities are of the order of 10 %.

The Navier–Stokes equations are solved on a cubic grid of size N^3 for $N = 128, 256, 512$ with periodic boundary conditions. Energy is injected by keeping constant the spectral content of the two smallest-wavenumber shells (Chen *et al.* 1993). The viscosity is chosen so to have a Kolmogorov lengthscale $\eta \approx \Delta x$ where Δx is the grid spacing: this choice ensures a good resolution of the small-scale velocity dynamics. We use a fully dealiased pseudospectral algorithm with second-order Adam–Bashforth time-stepping. The Reynolds numbers achieved are in the range $R_\lambda \in [65:185]$.

The equations of fluid motion are integrated until the system reaches a statistically steady state. Then, particles are seeded with homogeneously distributed initial positions and velocities equal to the local fluid velocity. Equations (2.1) and (2.2) are then advanced in parallel. A transient in particle dynamics follows, for about 2–3 large-scale eddy turnover times, before reaching Lagrangian stationary statistics. It is only after this relaxation stage has completely elapsed that the measurement starts. We followed 15 sets of inertial particles with Stokes numbers from 0.16 to 3.5. For each set, we saved the position and the velocity of N_t particles every $\mathrm{d}t = 1/10\tau_\eta$ with a maximum number of recorded trajectories of $N_t = 5\times10^5$ for the highest resolution. Along these trajectories we also stored the velocity of the carrier fluid. At a lower frequency $\sim 10\tau_\eta$, we saved the positions and velocities of a larger number N_p of particles (up to 7.5×10^6 per St at the highest resolution) together with the Eulerian velocity field. We have also followed fluid tracers ($St = 0$), that evolve according to the dynamics

$$\frac{\mathrm{d}\boldsymbol{x}(t)}{\mathrm{d}t} = \boldsymbol{u}(\boldsymbol{x}(t), t), \tag{2.3}$$

in order to systematically assess the importance of the phenomenon of preferential concentration at varying both St and R_λ.

A summary of the various physical parameters is given in table 1.

3. Results and discussion

In this paper we focus on the statistics of particle acceleration $\boldsymbol{a}(t) = \mathrm{d}\boldsymbol{V}/\mathrm{d}t$. From previous studies on fluid tracers we know that acceleration statistics are very intermittent and strong fluctuations are associated with trapping events within vortex filaments (La Porta *et al.* 2001, 2002; Mordant *et al.* 2001; Biferale *et al.* 2005). How does inertia affect acceleration statistics? A good starting point to gain insight into the effect of inertia is given by the formal solution of (2.1) in the statistically

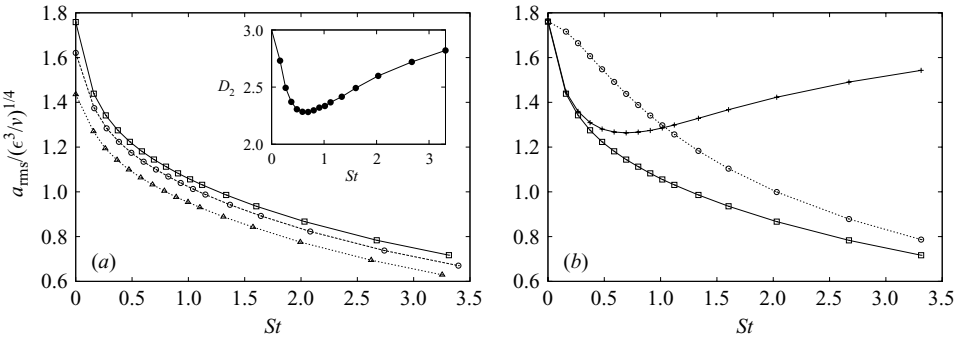

FIGURE 1. (*a*) The normalized acceleration variance $a_{\rm rms}/(\epsilon^3/\nu)^{1/4}$ as a function of the Stokes number for $R_\lambda = 185$ (□); 105 (○); 65 (△). The inhomogeneous distribution of particles is quantified for the highest R_λ in the inset, where we plot the correlation dimension, D_2, as a function of St. The correlation dimension is defined as $p(r) \sim r^{D_2}$ (for $r \ll \eta$) where $p(r)$ is the probability of finding two particles closer than r (Bec *et al.* 2005). (*b*) Comparison between the acceleration variance, $a_{\rm rms}$ (□), as a function of St, with the acceleration of the fluid tracer measured at the particle position, $\langle(\mathrm{D}\boldsymbol{u}/\mathrm{D}t)^2\rangle^{1/2}$ (+). The curve (○), approaching the $a_{\rm rms}$ for large St, is the one obtained from the filtered tracer trajectories, $a^F_{\rm rms}$. All data refer to $Re_\lambda = 185$.

stationary state, relating the instantaneous particle velocity to the previous history of fluid velocity along the particle trajectory. It is expressed as

$$\boldsymbol{V}(t) = \frac{1}{\tau_s}\int_{-\infty}^{t} \mathrm{e}^{-(t-s)/\tau_s}\boldsymbol{u}(\boldsymbol{X}(s), s)\,\mathrm{d}s \tag{3.1}$$

yielding for the acceleration

$$\boldsymbol{a}(t) = \frac{1}{\tau_s^2}\int_{-\infty}^{t} \mathrm{e}^{-(t-s)/\tau_s}[\boldsymbol{u}(\boldsymbol{X}(t), t) - \boldsymbol{u}(\boldsymbol{X}(s), s)]\,\mathrm{d}s. \tag{3.2}$$

It is instructive to analyse separately the two limiting cases of small and large Stokes numbers.

At small St, i.e. $\tau_s \ll \tau_\eta$, the fluid velocity along the trajectory evolves smoothly in time and expression (3.2) for the acceleration reduces to $\boldsymbol{a}(t) \simeq (\mathrm{d}/\mathrm{d}t)\boldsymbol{u}(\boldsymbol{X}(t), t)$, i.e. to the derivative of fluid velocity along the inertial particle trajectory. At sufficiently small St this is indistinguishable from the fluid acceleration $(\mathrm{D}\boldsymbol{u}/\mathrm{D}t)(\boldsymbol{X}(t), t)$ evaluated at the particle positions. The latter, in turn, is essentially dominated by the $-\boldsymbol{\nabla}p$ contribution. Therefore we can draw the following picture for the small-St case: the heavy particle acceleration essentially coincides with the fluid acceleration; however, inertial particles are not homogeneously distributed in the flow and concentrate preferentially in regions with relatively small pressure gradient (low-vorticity regions). As a result, the net effect of inertia is a drastic reduction of the root-mean-squared acceleration $a_{\rm rms} = \langle \boldsymbol{a}^2\rangle^{1/2}$, due essentially to preferential concentration. Indeed, as shown in figure 1(*a*) the acceleration variance has already droped off very fast at quite small St values. In figure 1(*b*) we give evidence that the value of $a_{\rm rms}$ is very close to $\langle(\mathrm{D}\boldsymbol{u}/\mathrm{D}t)^2\rangle^{1/2}$ for $St < 0.4$ when the average is not taken homogeneously in space but conditioned at be on the same spatial positions as the inertial particles. The agreement of the two curves supports the arguments above. Notice that for increasing St the two curves start to deviate from each other, the tracer acceleration conditioned on the particle positions has a minimum for $St \approx 0.5$ close to the maximum of clustering

(see inset of figure 1*a*), eventually recovering the value of $a_{\rm rms}$ of the unconditioned tracers for larger St. The latter effect is a clear indication that inertial particles follow the small-scale structures of the flow more and more homogeneously on increasing St. In this limit a different mechanism is responsible for the reduction of the $a_{\rm rms}$.

At large St, i.e. $\tau_s \gg \tau_\eta$, inspection of (3.2) shows that the main effect of inertia on particle acceleration is a low-pass filtering of fluid velocity differences, with a suppression of fast frequencies above τ_s^{-1}. In figure 1(*b*) we also compare the acceleration variance with that obtained by an artificial low-pass filtering based only on the fluid tracer trajectories. For each tracer trajectory, $\boldsymbol{x}(t)$, we define a new velocity, $\boldsymbol{u}^F$, filtered on a window size of the same order as the Stokes time:

$$\boldsymbol{u}^F(t) = \frac{1}{\tau_s}\int_{-\infty}^{t} \mathrm{e}^{-(t-s)/\tau_s}\boldsymbol{u}(\boldsymbol{x}(s), s)\,\mathrm{d}s. \tag{3.3}$$

The filtered acceleration is thus given by $\boldsymbol{a}^F = (\mathrm{d}/\mathrm{d}t)\boldsymbol{u}^F$. Of course, in order to extract the effect due to filtering only we need to employ fluid trajectories: (3.3) applied along particle trajectories is the same as (3.1), so that the acceleration would coincide with the particle acceleration by definition. The root mean square fluctuation, $a^F_{\rm rms} = \langle(\mathrm{d}/\mathrm{d}t)\boldsymbol{u}^F)^2\rangle^{1/2}$, is thus computed by averaging along the tracer trajectories without any condition on their spatial positions, i.e. homogeneously distributed in the whole three-dimensional domain. The curves corresponding to $a_{\rm rms}$ and to $a^F_{\rm rms}$ become closer and closer together as St increases, supporting the conjecture that preferential concentration for $St > 1$ becomes less important. For intermediate St we expect a non-trivial interplay between the two above mechanisms that makes it very difficult to build up a model able to reproduce even the qualitative behaviour.

Another interesting aspect shown in figure 1(*a*) is the residual dependence of the normalized particle acceleration on Reynolds number. For the case of fluid tracers it is known that intermittent corrections to the dimensional estimate $a_{\rm rms} = a_0(\epsilon^3/\nu)^{1/4}$ may explain the Reynolds number dependence (Sawford *et al.* 2003; Hill 2002; Biferale *et al.* 2004). Data suggest that the fluid intermittency may be responsible of such deviations at $St > 0$ as well. This view is supported by the fact that the curves for the three Reynolds numbers are almost parallel.

A two-parameter formula for the variance of the acceleration as a function of Stokes number can be derived in the limit of vanishing Stokes numbers: $a^2_{\rm rms}(St) = a^2_{\rm rms}(0) + C\exp[-(D/St)^\delta]$ (G. Falkovich 2005, personal communication). This expression follows from the acceleration probability distribution function (p.d.f.) of tracer particles under the assumptions that (i) the main effect of inertia is to reduce the particle concentration in regions where the acceleration is larger than $\nu^{1/2}/{\tau_s}^{3/2}$; (ii) the p.d.f. tail is well reproduced by a stretched exponential shape with exponent $\beta = 2/3\delta$. Although the formula fits the data well, the limitation of our data-set to only a few points with $St \ll 1$ does not permit a significant benchmark of the model.

In table 2 we summarize the values that we have measured for $\langle\boldsymbol{a}^2\rangle$ and $\langle\boldsymbol{a}^4\rangle$ as a function of all Stokes numbers and for all Reynolds numbers available. Besides the effect of inertia on typical particle acceleration it is also interesting to investigate the effects on the form of the p.d.f. $\boldsymbol{a}(t)$. As shown in figure 2(*a*), the p.d.f.s become less and less intermittent as St increases. In the inset of the same figure we show the flatness, $\langle\boldsymbol{a}^4\rangle/\langle\boldsymbol{a}^2\rangle^2$, as a function of St. The abrupt decreasing for $St > 0$ is even more evident here (notice that the y scale is logarithmic).

In the limits of small and large St the qualitative trend of the p.d.f.s can be captured by the same arguments used for $a_{\rm rms}$. In figure 2(*b*) we compare the p.d.f. shape for

(*a*)	St	0	0.16	0.27	0.37	0.48	0.59	0.69	0.80	0.91	1.01	1.12	1.34	1.60	2.03	2.67	3.31
	$\langle\tilde{a}^2\rangle$	3.09	2.07	1.80	1.63	1.50	1.39	1.31	1.24	1.17	1.12	1.06	0.97	0.88	0.75	0.61	0.51
	$\langle\tilde{a}^4\rangle$	288	48.1	30.5	22.4	17.7	14.5	12.3	10.6	9.20	8.11	7.21	5.77	4.47	3.11	1.94	1.29
(*b*)	St	0	0.16	0.27	0.38	0.49	0.60	0.71	0.82	0.93	1.04	1.15	1.37	1.64	2.08	2.74	3.40
	$\langle\tilde{a}^2\rangle$	2.63	1.89	1.65	1.45	1.38	1.29	1.21	1.14	1.08	1.03	0.98	0.89	0.80	0.68	0.54	0.45
	$\langle\tilde{a}^4\rangle$	133	32.9	21.6	16.3	13.1	10.9	9.29	8.03	7.01	6.18	5.48	4.37	3.36	2.23	1.39	0.90
(*c*)	St	0	0.16	0.26	0.37	0.47	0.58	0.68	0.79	0.89	1.00	1.10	1.31	1.57	1.99	2.62	3.25
	$\langle\tilde{a}^2\rangle$	2.02	1.59	1.40	1.28	1.19	1.11	1.05	0.99	0.94	0.89	0.85	0.77	0.70	0.59	0.47	0.39
	$\langle\tilde{a}^4\rangle$	52.8	19.1	13.1	10.1	8.24	6.95	6.01	5.24	4.61	4.11	3.67	2.95	2.32	1.59	0.97	0.63

TABLE 2. Normalized values of the second and fourth moments of the acceleration $\langle\tilde{a}^2\rangle = \langle\boldsymbol{a}^2\rangle/[3(\epsilon^3/\nu)^{1/2}]$, $\langle\tilde{a}^4\rangle = \langle\boldsymbol{a}^4\rangle/[3(\epsilon^3/\nu)]$ for (*a*) $R_\lambda = 185$, (*b*) $R_\lambda = 105$ and (*c*) $R_\lambda = 65$. The statistical error on all entries are of the order of 5 %.

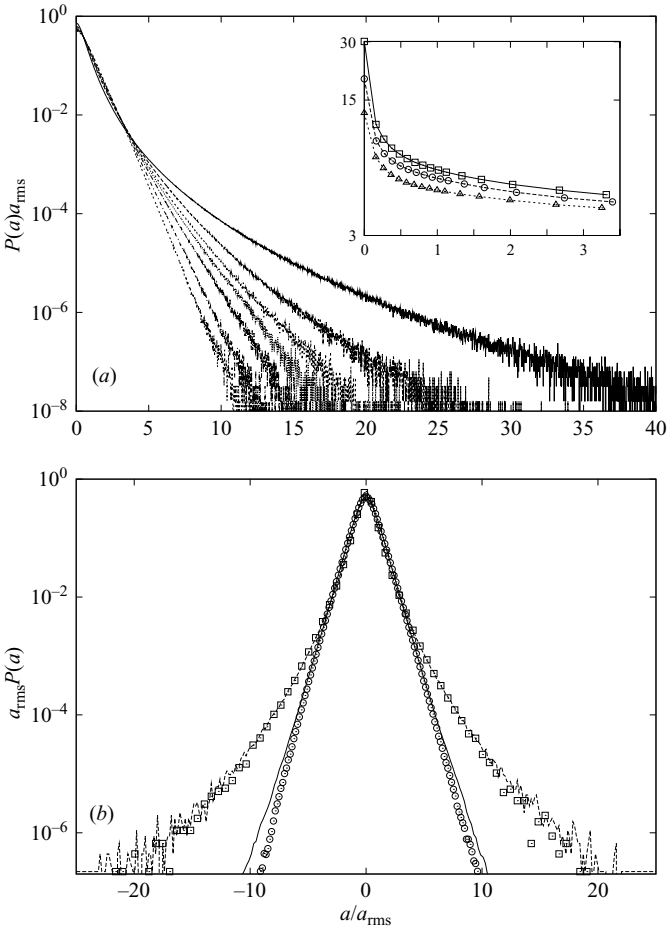

FIGURE 2. (*a*) Acceleration p.d.f.'s for a subset of St values ($St = 0, 0.16, 0.37, 0.58, 1.01, 2.03, 3.31$ from top to bottom) at $R_\lambda = 185$. The inset displays the acceleration flatness, $\langle\boldsymbol{a}^4\rangle/\langle\boldsymbol{a}^2\rangle^2$, at increasing R_λ from bottom to top. (*b*) The two outer curves correspond to the acceleration p.d.f. for $St = 0.16$ (□) and the p.d.f. of the fluid tracers acceleration measured at the same position of the inertial particles, $\mathrm{D}\boldsymbol{u}/\mathrm{D}t$ (dashed line). The two inner curves are the acceleration p.d.f. at the highest Stokes, $St = 3.31$ (○) and the p.d.f. of the filtered fluid acceleration (solid line). All curves are normalized to have unit variance.

the smallest Stokes number with the one obtained by using the tracer acceleration measured on the particle position, $\mathrm{D}\boldsymbol{u}/\mathrm{D}t$. The two functions overlap perfectly, confirming that the only difference between fluid particles and inertia particles for small St is due to preferential concentration. In the same figure we also compare, for the highest Stokes number, $St = 3.31$, the p.d.f. of the particle acceleration with the one obtained from the filtered fluid trajectories. Now the agreement is less perfect but still fairly good, providing reassurance that this limit can be captured starting from a low-pass filter of fluid tracer velocities. Note that the p.d.f. of tracer acceleration measured on the particle position, $\mathrm{D}\boldsymbol{u}/\mathrm{D}t$, approaches the unconditioned p.d.f. as St increases (not shown). This further confirms that preferential concentration plays a minor role in the acceleration at these large Stokes numbers.

4. Statistics of acceleration conditioned on the flow topology

We now focus on particle acceleration statistics conditioned on the topological properties of the carrier flow at the particle positions. In particular, we look at the sign of the discriminant (see e.g. Chong, Perry & Cantwell 1990 and Bec 2005):

$$\Delta = \left(\frac{\det[\hat{\boldsymbol{\sigma}}]}{2}\right)^2 - \left(\frac{\mathrm{Tr}[\hat{\boldsymbol{\sigma}}^2]}{6}\right)^3, \tag{4.1}$$

where $\hat{\sigma}_{ij} = \partial_i u_j$ is the strain matrix evaluated at the particle position $\boldsymbol{X}$. Note that, in deriving (4.1), we omitted the term proportional to $\mathrm{Tr}[\hat{\boldsymbol{\sigma}}]$ because of incompressibility. For $\Delta \leqslant 0$ the strain matrix has three real eigenvalues (strain-dominated regions); for $\Delta > 0$ it has a real eigenvalue and two complex conjugate ones (rotational regions). For a similar study, using a different different characterization of the flow structures, see (Squires & Eaton 1991). Note that in two dimensions the equivalent of Δ is the well-known Okubo–Weiss parameter that differentiates elliptic from hyperbolic regions of the flow.

In figure 3(*a–c*) we show the acceleration p.d.f., $P(a|\Delta)$, conditioned on the sign of Δ at particle positions, for three different characteristic Stokes number $St = 0.16, 0.48, 1.34$. In figure 3(*d*) we show the root-mean-squared acceleration, $\sqrt{\langle a^2|\Delta\rangle/3}$, as a function of St. A few results are worth noting. The fraction of particles in the two regions ($N(\Delta \gtrless 0)$) varies considerably as a function of the Stokes number (see inset of figure 3*d*), with a depletion of particles in the regions with some degree of rotation, which becomes less effective at large St. This is similar to what is observed in the inset of figure 1(*a*), where the non-homogeneous particle distribution is characterized in terms of the correlation dimension (Bec *et al.* 2005). Further, although the shape of the p.d.f. for a given Stokes number does not change much as a function of the sign of Δ, a noticeable change in the squared acceleration is observed. As shown in figure 3(*d*), the acceleration is higher in the strain-dominated regions than in the ones with some degree of rotation. Note that the effect of inertia is dramatic: for the smallest St the conditional acceleration is larger when $\Delta < 0$ while the opposite behaviour is observed for tracer ($St = 0$). This may be the signature of the expulsion of particles out of intense vortex filaments (which is more effective for $St \ll 1$) leading to an undersampling of the acceleration in the regions dominated by rotational motion. The same difference is also measured for higher moments of the conditioned acceleration (not shown).

These results show that the strong correlation between flow structure and particle preferential concentration is more effective at low Stokes numbers. At larger St the particle fraction $N(\Delta \gtrless 0)$ approaches the tracer value (the response time is too large to maintain the correlation between particle trajectories and the local flow topology)

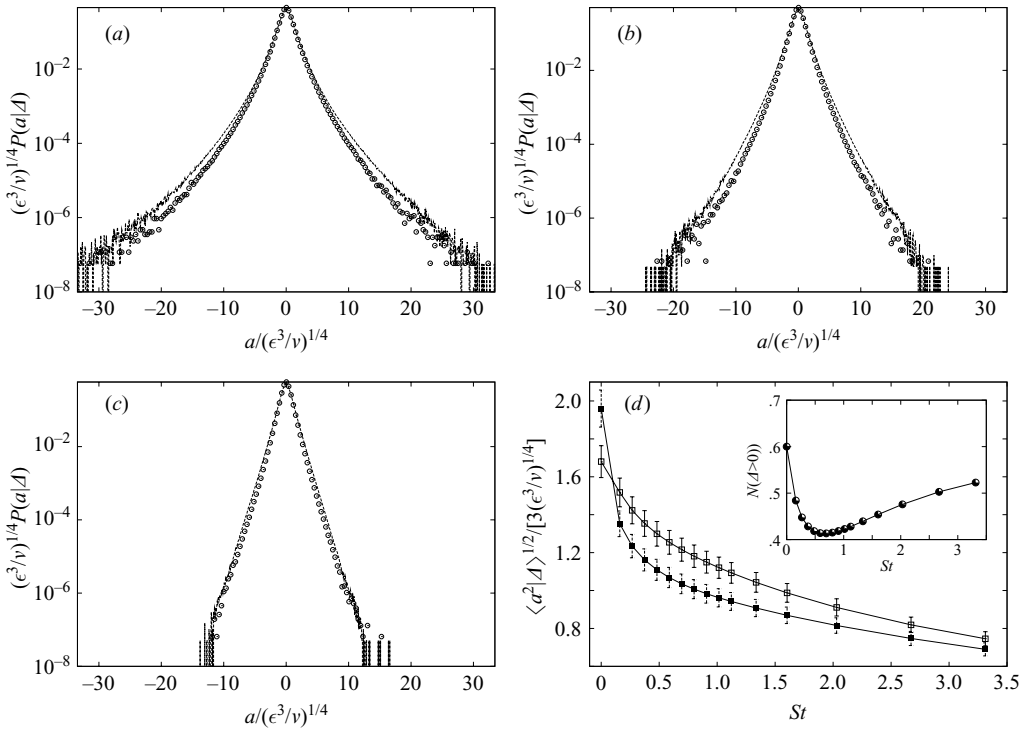

FIGURE 3. (*a–c*) Acceleration statistics conditioned on the sign of the discriminant Δ defined in (4.1). (*a*) P.d.f.s of acceleration for (*a*) $St = 0.16$, (*b*) 0.48, (*c*) 1.34, conditioned on strain regions (solid line, $\Delta \leqslant 0$) and on rotating regions (symbols, $\Delta > 0$) regions, respectively. (*d*) Normalized root mean square conditional acceleration on $\Delta \leqslant 0$ (open squares) and $\Delta > 0$ (filled squares) regions as a function of St. The inset displays the fraction of particles in the rotating regions $N(\Delta > 0)$ ($N(\Delta \leqslant 0) = 1 - N(\Delta > 0)$) as a function of St. The conditional acceleration was computed on the data recorded at frequency $10\tau_\eta$ (see table 1). For $St = 0$ the acceleration $\sqrt{\langle a^2|\Delta\rangle/3}$ is estimated using the pressure gradient $-\nabla p$.

and the depletion of acceleration should be ascribed to the effect of filtering, as discussed in the previous section (cf. figures 1*b* and 2*b*).

5. Conclusions and perspectives

A systematic study of the acceleration statistics of heavy particles in turbulent flows, on changing both Stokes and Reynolds numbers has been presented. The main conclusions are (i) preferential concentration plays an almost singular role at small St. Indeed, even a quite small inertia may suffice to expel particles from those turbulent regions (vortex cores) where the most intermittent and strong acceleration fluctuations would be experienced; (ii) for small St, a good quantitative agreement between the inertial particle acceleration and the conditioned fluid tracer acceleration is obtained; (iii) at large St, the main effect is filtering of the velocity induced by the response Stokes times. For $St > 1$, the statistical properties of fluid tracers averaged over a time window of the order of τ_s are in quite good agreement with the inertial particle properties.

Some important questions remain open. It is not clear how to build up a phenomenological model that is able to describe the inertial particle acceleration as a

function of both Stokes and Reynolds numbers. For example, a naive generalization of the multifractal description, successfully used for fluid tracers (Biferale *et al.* 2004), may be insufficient. It is not straightforward to include in such models the correlation between preferential concentration and the local topological properties of the carrier flow. Here such correlations have been studied in terms of the real or complex nature of the eigenvalues of the strain matrix at particle positions. We found that, more effectively at small rather than large St values, particles preferentially concentrate in strain-dominated regions and that this preferential concentration has a clear role in determining the acceleration fluctuations. However, this information does not directly lead to a model for the acceleration statistics.

The strong fluctuations of both Kolmogorov time and Kolmogorov dissipative scale are the most interesting aspects which distinguish the statistics of heavy particles in turbulence from those measured in smooth flows. It would thus be important to also study the statistical properties conditioned on the local Stokes number (defined in terms of a 'local' energy dissipation, see e.g. Collins & Keswani 2004).

Work in this direction will be reported elsewhere.

We acknowledge useful discussions with G. Falkovich, E. Bodenschatz and Z. Warhaft. This work was partially supported by the EU under the research training network HPRN-CT-2002-00300 "Stirring and Mixing". Numerical simulations were performed with the support of CINECA (Italy) and IDRIS (France) under the HPC-Europa project (R113-CT-2003-506079). We also thank the "Centro Ricerche e Studi Enrico Fermi" and N. Tantalo for support on the numerical computations.

REFERENCES

Balkovsky, E., Falkovich, G. & Fouxon, A. 2001 Intermittent distribution of inertial particles in turbulent flows. *Phys. Rev. Lett.* **86**, 2790–2793.

Bec, J. 2005 Multifractal concentrations of inertial particles in smooth random flows. *J. Fluid Mech.* **528**, 255–277.

Bec, J., Celani, A., Cencini, M. & Musacchio, S. 2005 Clustering and collisions of heavy particles in random smooth flows. *Phys. Fluids* **17**, 073301.

Bec, J., Gawedzki, K. & Horvai, P. 2004 Multifractal clustering in compressible flows. *Phys. Rev. Lett.* **92**, 224501.

Biferale, L., Boffetta, G., Celani, A., Devenish, B. J., Lanotte, A. & Toschi, F. 2004 Multifractal statistics of Lagrangian velocity and acceleration in turbulence. *Phys. Rev. Lett.* **93**, 064502.

Biferale, L., Boffetta, G., Celani, A., Lanotte, A. & Toschi, F. 2005 Particle trapping in three-dimensional fully developed turbulence. *Phys. Fluids* **17**, 021701.

Boffetta, G., De Lillo, F. & Gamba, A. 2004 Large scale inhomogeneity of inertial particles in turbulent flows. *Phys. Fluids* **16**, L20–L24.

Boivin, M., Simonin, O. & Squires, K. D. 1998 Direct numerical simulation of turbulence modulation by particles in isotropic turbulence. *J. Fluid Mech.* **375**, 235–263.

Chen, S., Doolen, G. D., Kraichnan, R. H. & She, Z. S. 1993 On statistical correlations between velocity increments and locally averaged dissipation in homogeneous turbulence. *Phys. Fluids* A **5**, 458-463.

Chong, M. S., Perry, A. E. & Cantwell, B. J. 1990 A general classification of three-dimensional flow field. *Phys. Fluids* A **2**, 765–777.

Chun, J., Koch, D. L., Rani, S., Ahluwalia, A. & Collins, L. R. 2005 Clustering of aerosol particles in isotropic turbulence. *J. Fluid Mech.* **536**, 219–251.

Collins, L. R. & Keswani, A. 2004 Reynolds number scaling of particle clustering in turbulent aerosols. *New J. Phys.* **6**, 119.

Csanady, G. 1980 *Turbulent Diffusion in the Environment*. D. Reidel.

Eaton, J. K. & Fessler, J. R. 1994 Preferential concentrations of particles by turbulence. *Intl J. Multiphase Flow* **20**, 169–209.

Falkovich, G., Fouxon, A. & Stepanov, M. 2002 Acceleration of rain initiation by cloud turbulence. *Nature* **419**, 151–154.

Falkovich, G. & Pumir, A. 2004 Intermittent distribution of heavy particles in a turbulent flow. *Phys. Fluids* **16**, L47–L51.

Hill, R. J. 2002 Scaling of acceleration in locally isotropic turbulence. *J. Fluid Mech.* **452**, 361–370.

La Porta, A., Voth, G. A., Crawford, A. M., Alexander, J. & Bodenschatz, E. 2001 Fluid particle accelerations in fully developed turbulence. *Nature* **409**, 1017–1019.

La Porta, A., Voth, G. A., Crawford, A. M., Alexander, J. & Bodenschatz, E. 2002 Measurement of particle accelerations in fully developed turbulence. *J. Fluid Mech.* **469**, 121–160.

Lewis, D. & Pedley, T. 2000 Planktonic contact rates in homogeneous isotropic turbulence: Theoretical predictions and kinematic simulations. *J. Theor. Biol.* **205**, 377–408.

Maxey, M. R. & Riley, J. 1983 Equation of motion of a small rigid sphere in a nonuniform flow. *Phys. Fluids* **26**, 883–889.

Mordant, N., Metz, P., Michel, O. & Pinton, J.-P. 2001 Measurement of Lagrangian velocity in fully developed turbulence. *Phys. Rev. Lett.* **87**, 214501.

Pinsky, M. & Khain, A. 1997 Turbulence effects on droplet growth and size distribution in clouds–a review. *J. Aerosol Sci.* **28**, 1177–1214.

Post, S. & Abraham, J. 2002 Modeling the outcome of drop-drop collisions in Diesel sprays. *Intl J. Multiphase Flow* **28**, 997–1019.

Reade, W. C. & Collins, L. R. 2000 A numerical study of the particle size distribution of an aerosol undergoing turbulent coagulation. *J. Fluid Mech.* **415**, 45–64.

Rothschild, B. J. & Osborn, T. R. 1988 Small-scale turbulence and plankton contact rates. *J. Plankton Res.* **10**, 465–474.

Sawford, B. L. & Guest, F. M. 1991 Lagrangian statical simulation of the turbulent motion of heavy particles. *Boundary-Layer Met.* **54**, 147–166.

Sawford, B. L., Yeung, P. K., Borgas, M. S., Vedula, P., La Porta, A., Crawford, A. M. & Bodenschatz, E. 2003 Conditional and unconditional acceleration statistics in turbulence. *Phys. Fluids* **15**, 3478–3489.

Seinfeld, J. 1986 *Atmospheric Chemistry and Physics of Air Pollution*. J. Wiley and Sons.

Shaw, R. A. 2003 Particle-turbulence interactions in atmospheric clouds. *Annu. Rev. Fluid Mech.* **35**, 183–227.

Squires, K. D. & Eaton, J. K. 1991 Preferential concentration of particles by turbulence. *Phys. Fluids* A **3**, 1169–1178.

Villedieu, P. & Hylkema, J. 2000 Modèles numériques lagrangiens pour la phase dispersée dans les propulseurs à poudre. *Rapport technique ONERA*.

Warhaft, Z., Gylfason, A. & Ayyalasomayajula, S. 2005 private communication.

Zaichik, L. I., Simonin, O. & Alipchenkov, V. M. 2003 Two statistical models for predicting collision rates of inertial particles in homogeneous isotropic turbulence. *Phys. Fluids* **15**, 2995–3005.

Zhou, Y., Wexler, A. & Wang, L.-P. 2001 Modelling turbulent collision of bidisperse inertial particles. *J. Fluid Mech.* **433**, 77–104.